JOURNAL OF MATERIALS SCIENCE 19 (1984) 377–384

Failure modes and fracture mechanisms in flexure of Kevlar–epoxy composites

M. DAVIDOVITZ*, A. MITTELMAN†, I. ROMAN†, G. MAROM*
The Casali Institute of Applied Chemistry and Materials Science Division†, School of Applied Science and Technology, The Hebrew University of Jerusalem, 91904 Jerusalem, Israel*

The results of testing in three-point bending of aramid fibre-reinforced epoxy composites are described. This loading mode has been chosen in order to increase the variety of failure modes and of fracture mechanisms. The main failure modes observed are tensile and delamination, with a transition at a fibre volume fraction of about 46%. This mode transition is detectable by monitoring various mechanical properties and acoustic emission data against the fibre volume fraction. The tensile mode comprises a fracture mechanism of fibre splitting and pull-out and the delamination comprises fibre bending, tearing off of fibre skin and shearing of individual filaments. Other effects such as the shifting of the neutral axis and the compressive failure at the compression side are also reported.

1. Introduction

The steadily increasing utilization of Kevlar 49, poly (*p*-phenylene terephthalamide) (PPTA) fibres in high performance composite materials for structural applications demands that reliable quality control techniques be developed. Usually, the establishment of such a technique is a two-stage process consisting of a systematic identification of the fundamental failure processes and relevant defects, followed by correlating a particular non-destructive output with a specific defect or mechanism.

Such an approach was practiced in the present study whose ultimate goal has been to develop a non-destructive procedure for the evaluation of filament-wound pressure vessels. One of the techniques chosen for investigation and reported below was based on acoustic emission. Accordingly, the initial task was to identify the overall failure modes and the actual microscopic and macroscopic fracture mechanisms in PPTA fibre-reinforced composites, and to correlate them with acoustic emission events occurring during the loading of the composites – both before and during the occurrence of the major failure event.

In view of the need to characterize a variety as wide as possible of fracture mechanisms testing was carried out in flexure. This is a more versatile loading configuration whereby three major failure modes may be induced, namely, tensile, compressive and delamination, each comprising a sequence of fracture events.

In the text below we discuss in detail the observed fracture mechanisms and failure modes, while the acoustic emission data are presented only briefly; a fuller account will be given elsewhere [1].

2. Experimental details

Composites of Kevlar 49 fibres – Araldite MY 750/HT 972 epoxy were manufactured from prepregs prepared in the laboratory by a fibre winding-impregnation technique. The complete manufacturing procedure was according to the reliable routine used for over 10 years with glass and graphite fibres (for details see for example [2]). The nominal thickness of the plates was 0.5 cm, and the test specimens were in the forms of 5.0 cm long bars 0.5 cm × 0.5 cm in cross-section. The exact fibre content of each plate was determined by the procedure given in [3]. Both interlaminar and translaminar specimens were tested.

0022–2461/84 $03.00 + .12

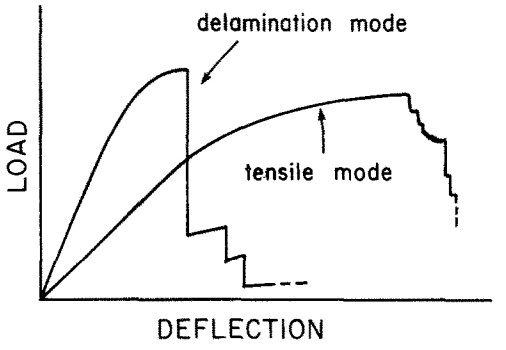

Figure 1 Typical load–deflection curves for the delamination and tensile failure modes.

Testing was carried out in 3-point bending with a loading span of 4.0 cm. Two acoustic emission resonant type transducers (175 and 375 kHz) were glued to the ends of the specimen by means of sticky wax which ensured impedance compatibility. The equipment comprised an Instron universal tester and an Acoustic Emission Technology AET-5000 system.

3. Results and discussion

The investigation of the fracture mechanism was performed on two levels. The first included fracture mechanisms responsible for the macroscopic failure of the material, and the second considered extraneous mechanisms and processes either resulting from the loading conditions or reflecting microscopic properties of the constituent materials.

3.1. Major modes of failure

The failure of Kevlar-reinforced epoxy composites in 3-point bending occurred by either one of two modes being failure by longitudinal fracture of fibres in the tensile side, or by shear delamination in the neutral plane. The first failure mode was typical of the lower volume fraction composites, and the second was typical of the higher, with a distinct transition in the volume fraction range 45–48%. With interlaminar loading the transition occurred at the lower end of the transition range, ~45%, and with translaminar loading the transition occurred at the higher end, ~48%.

Fig. 1 is a qualitative representation of the load–deflection curves for the respective failure modes. The curve of the fibre fracture mode is characterized by a yielding stage and a longer ultimate deflection. These result from compressive failure occurring in the compressive side of the specimen as discussed below. The curve of the delamination mode is characterized by a main delamination event followed by a number of secondary delaminations.

The transition from failure by fibre fracture to failure by delamination was determined by the fibre volume fraction. It was therefore detectable by monitoring various mechanical properties and plotting them against the fibre volume fraction. Figs. 2 to 4 present the transition as reflected by strength, energy and ultimate deflection measurements, respectively. The results show that under interlaminar loading the transition occurs around $\phi_f = 0.45$, and around $\phi_f = 0.48$ under translaminar. Although the ultimate strength values, σ, in Fig. 2 were calculated for the entire ϕ_f range, only those below the mode transition points are appropriate. Hence, in view of the observed transition to a delamination mode governed by the shear stress at the neutral plane, the ultimate shear strength values, τ, were calculated for ϕ_f values above the transition point. These are also shown in Fig. 2. The failure mode transition is also apparent in the values of the fracture energy to maximum load (Fig. 3), and in the values of the ultimate deflection (Fig. 4).

The reason for the mode transition at a critical

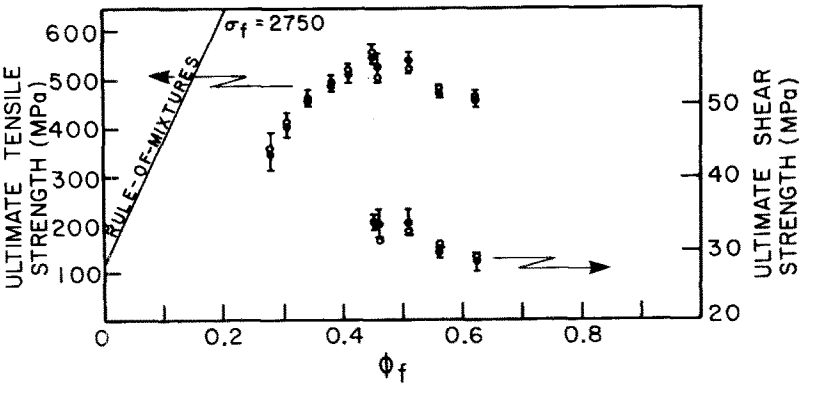

Figure 2 Ultimate tensile and shear strength values for interlaminar (•) and translaminar (○) loadings. The scatter bars belong to the interlaminar results.

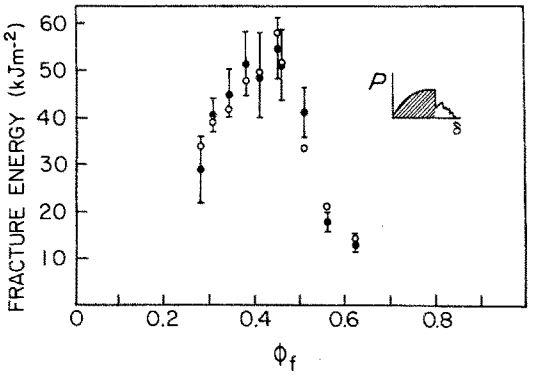

Figure 3 Fracture energy to maximum load for interlaminar (•) and translaminar (o) loadings. The scatter bars belong to the interlaminar results.

ϕ_f point probably lies with the different functions that σ and τ have in ϕ_f. Whereas σ increases linearly with ϕ_f, τ decreases due to increasingly high proportions of interface at the shear plane. In fact, at high ϕ_f values τ is governed by fibre–fibre contacts of zero strength and by the fibre–matrix interfacial strength being relatively weak with Kevlar fibres. Hence, the critical ϕ_f point is the value of ϕ_f for which σ and τ attain their ultimate values simultaneously. In the translaminar case τ may be higher due to the action of misaligned fibres, resulting in a somewhat higher critical ϕ_f.

Regarding the actual values of σ up to the transition point, they indeed seem to increase linearly with ϕ_f. However, they are smaller compared with the rule-of-mixtures values calculated with $\sigma_f = 2.75$ GPa. The lower values derived from a calculation assuming both tensile and compressive elastic behaviour of the Kevlar-reinforced composites. As a matter of fact these composites exhibit non-linear compressive behaviour, resulting in a stress distribution as shown in Fig. 5 [4]. It

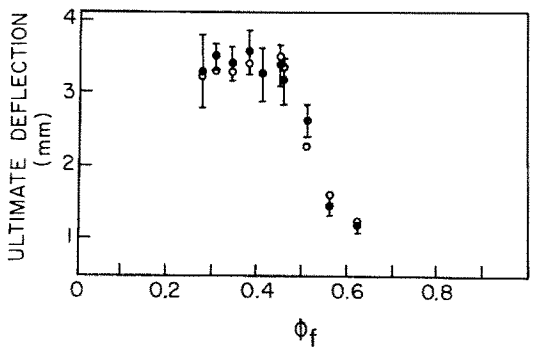

Figure 4 The ultimate deflection for interlaminar (•) and translaminar (o) loadings. The scatter bars belong to the interlaminar results.

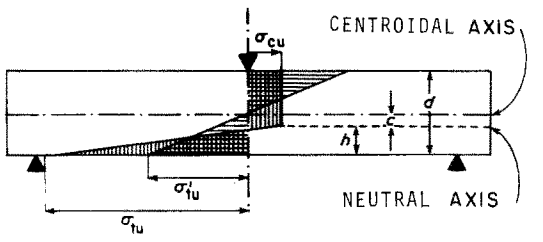

Figure 5 The shifting of the neutral axis for an elastic tensile/plastic compression behaviour.

shows the assumed stress distributions in the beam midspan cross-section as it is loaded to failure. The calculation of σ based on entirely elastic tensile/compressive behaviour yields an ultimate tensile strength value denoted by σ'_{tu} while the assumption of non-linear compressive behaviour yields a higher value denoted by σ_{tu} for an ultimate compressive strength σ_{cu}. Since we have been interested mostly in demonstrating the failure mode transition no further attempt has been made to calculate σ_{tu}, and the σ'_{tu} values are utilized in presenting that transition.

Another important outcome of the non-linear compressive behaviour is that stresses above the yield stress, $\sigma_y = \sigma_{cu}$, shift the neutral axis downward as shown in Fig. 5. The marking of this shifting is obtained when delamination failure occurs, taking place within the neutral plan in its ultimate new location away from the centroidal axis. This is shown in Fig. 6 with four specimens representing different fibre volume fractions above the critical ϕ_f, which sets the failure mode transition. The fibre volume fraction of each specimen is also indicated, and it is seen that the ultimate displacement of the neutral plan decreases as the fibre volume fraction increases. According to [4] the displacement c (Fig. 5) is given by

$$\frac{c}{d} = \frac{1-r+r^2}{2(1+r)^2} \tag{1}$$

where $r = \sigma_t/\sigma_y$. Since $\sigma_y = \sigma_{cu} =$ constant and σ_t, the tensile stress, increases with the applied load, consequently r and concomitantly c/d increase also. At the onset of delamination c achieves its ultimate value, yet $\sigma_t < \sigma_{tu}$, otherwise failure would have occurred in the tensile mode. Regarding the observed decrease in c/d with ϕ_f (Fig. 6), it is maintained that since the ultimate shear stress reduces with ϕ_f, the ultimate beam deflection, and in turn the tensile stress, diminish, producing smaller and smaller displacements of the neutral plan.

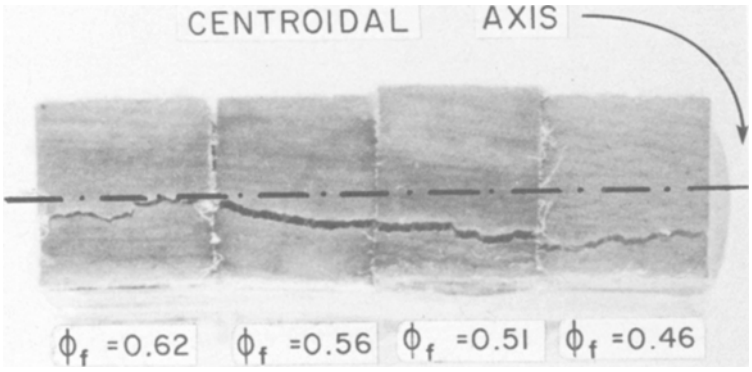

Figure 6 The displacement of the neutral plane (marked by delamination) from the centoidal plane as affected by the fibre volume fraction.

The values of τ calculated for the delamination mode (Fig. 2) extrapolate to about 30 MPa for $\phi_f = 0.79$ (assuming a square array of fibres). This 50% reduction in τ with respect to the shear strength of the resin (65 MPa) results from increasingly higher proportions of weak interface and fibre–fibre contact points in the shear plane as ϕ_f is increased. It corresponds very well with results in the literature of ~34 MPa for ϕ_f of about 60% [5, 6], and with a value of 34.8 MPa calculated on the basis of single filament pull-out experiments [7].

3.2. Fractography

Fractographic examinations of the fractured specimens revealed typical features of the two observed modes of failure. Fig. 7 contains a sequence of scanning fractographs showing the details of a tensile failure mode. The important observation concerns the fracture of the PPTA fibres and their pull-out from the fractured matrix. It is seen that the fracture of the Kevlar fibres occurs through an axial splitting mechanism, followed by a pull-out stage of the two opposing split portions. The splitting characteristics have been described before by other investigators [8, 9], and its mechanism has recently been attributed to the micro-structure of the PPTA fibres, comprising highly oriented fibrillar skin encasing a crystalline core consisting of row lamellae [10]. Such a micro-structure explains the fibre fracture mechanism, which involves transverse core failure at the weakest internal defect planes, skin failure at different points along the fibre in the region of these planes, and interconnection of the core defect planes and failed skin points by longitudinal crack propagation along the core-skin interface.

The details of the delamination failure mode are presented in Fig. 8 by a sequence of scanning electron fractographs showing the origination of

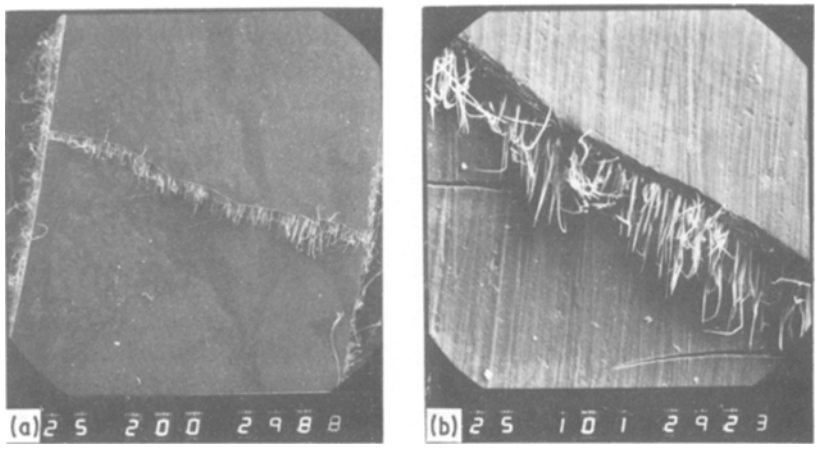

Figure 7 A sequence of scanning electron fractographs of the tensile side of the specimen showing details of a tensile failure mode.

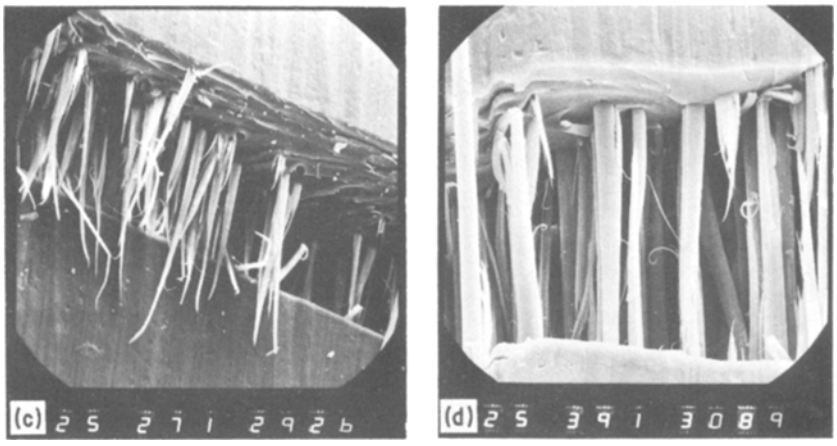

Figure 7 Continued.

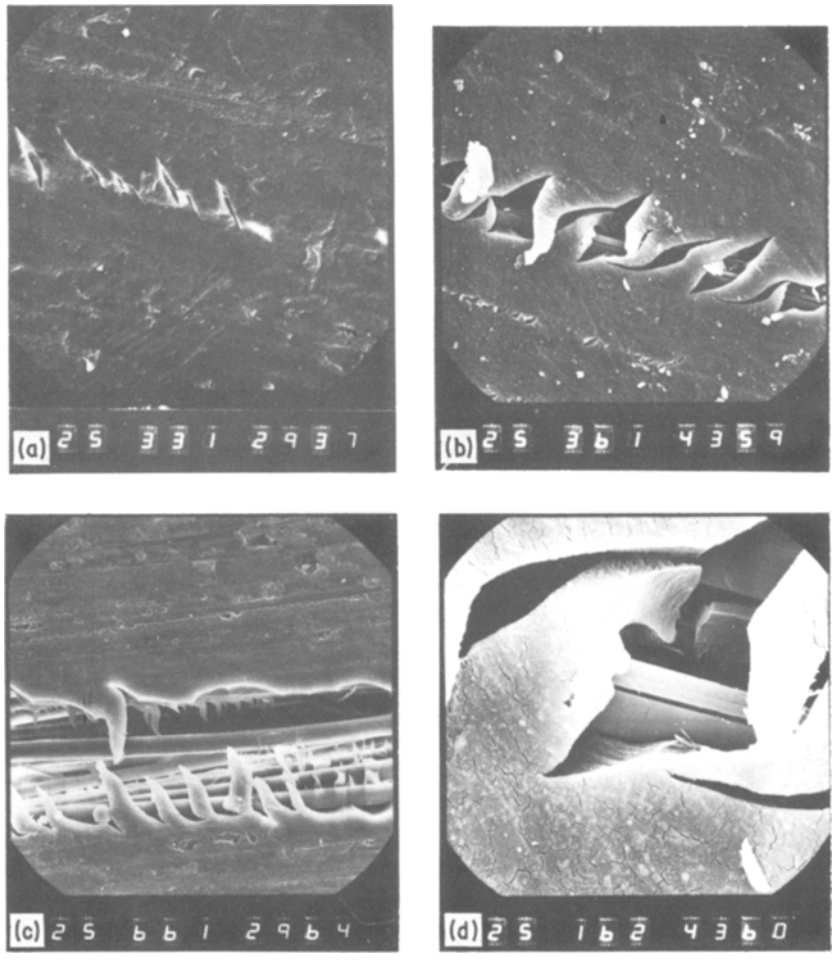

Figure 8 A sequence of scanning electron fractographs of the side of the specimen showing details of a delamination failure mode.

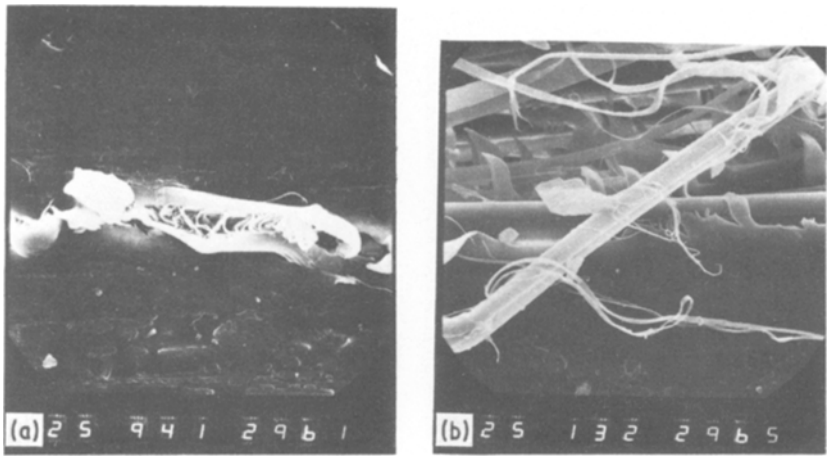

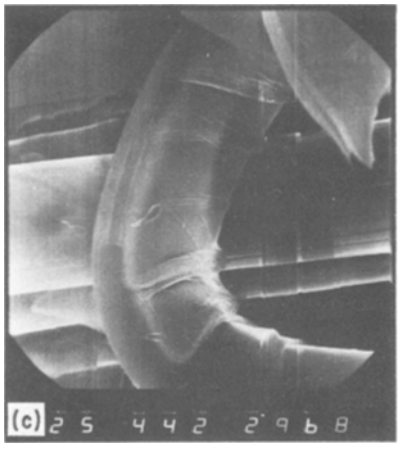

Figure 9 Typical fibre failure events occurring during delamination: (a) Shearing of an individual filament; (b) Tearing-off of fibre skin; (c) Deformation bands on a sharp bend.

delamination, the initial formation of shear bands in the matrix, the final shear damage in the matrix typical of the delamination mode, and the typical splitting of the fibre. Although fibre splitting occurs under both tensile and delamination failure modes, fracture proceeds differently in each case. Fig. 9 presents three typical fibre failure events under the delamination mode. The most interesting and unique is the shear failure of an individual filament seen in Fig. 9a. The other two events are the tearing-off in the axial direction of the fibre kin to form a continuous ribbon [9], and the production of deformation bands on the compression side of a sharp bend [11, 12], where a clean naked fibre just protrudes from the delamination plane.

Figure 10 Damage induced by the central loading roller. The fibre volume fraction of the specimens increases upward.

3.3. Extraneous effects

Under the title of extraneous effects we list types of damage which are not related directly to the two major failure modes. One such damage is related to the local effect of the central loading roller. It is seen in Fig. 10, where two effects are prominent. The first is the actual indentation of the specimen by the roller, and the second is some related damage in the vicinity of the indentation. The size of the second damage type decreases with the fibre volume fraction, and it is attributed to micro-cracking of the matrix as seen in Fig. 11. In addition, Fig. 11 presents the type of matrix damage observed in the tensile side under tensile failure mode. This is in agreement with obser-

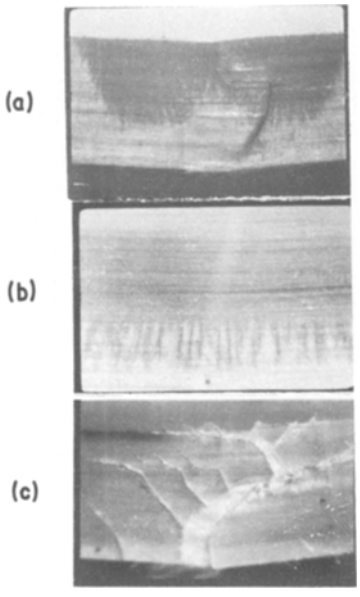

Figure 11 Micro-cracking of the matrix under the central loading roller (a, b); and the matrix cracking at the side of the specimen under the tensile failure mode (c).

vations in the literature [13]. The interaction of the regional stress field induced by the loading roller with the compressive stress field is expected to shift the neutral plane upward [14]. However, the effect of elastic tensile and plastic compressive behaviours dominates, resulting in a net displacement of the neutral plane downward, as described in Section 3.1.

Another damage which appears in the vicinity of the loading roller is the development of diagonal kink (shear) bands. These are shown in Fig. 12, and it is observed that when two such kink bands cross one another they form an initiation site for delamination in a plane perpendicular to the neutral plane. The source of these kink bands is the compressive stress in that side of the specimen near the loading roller. They have been observed in other composite systems such as glass and graphite fibre-reinforced resins [15–17], and several models have been proposed for the angle which they form with the fibre direction [15, 18]. The mechanism of their formation in PPTA fibre is different though. Whereas in graphite fibre composites, for instance, the kink bands comprise broken pieces of fibres, in PPTA fibres they consist of an assembly of kink bands in the individual filaments caused by the unique compression behaviour of the PPTA fibres [9, 17]. The angles of the kink bands as measured in the present study were in the range 45–50° C, which does not correspond with the angle calculated on the basis of the model in [18] for CFRP.

3.4. Acoustic emission

The traditional acoustic emission characterization techniques, i.e. counting and r.m.s. intensities were found to be insensitive to the failure mode transition described above. However, amplitude distribution characteristics showed a distinct transition at $\phi_f \approx 0.5$. This is seen by comparing between Figs. 13a and b, which contain typical amplitude distributions obtained for samples of $\phi_f = 0.38$ and $\phi_f = 0.56$, where tensile and delamination failure modes occurred, respectively. It is evident

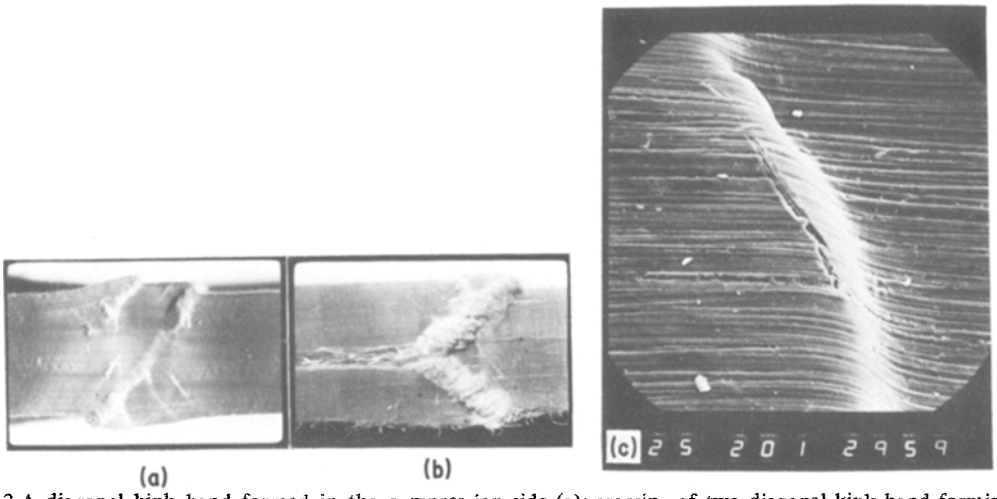

Figure 12 A diagonal kink band formed in the compression side (a); crossing of two diagonal kink band forming an initiation site for delamination (b); a scanning electron micrograph of a kink band view at the side of the specimen.

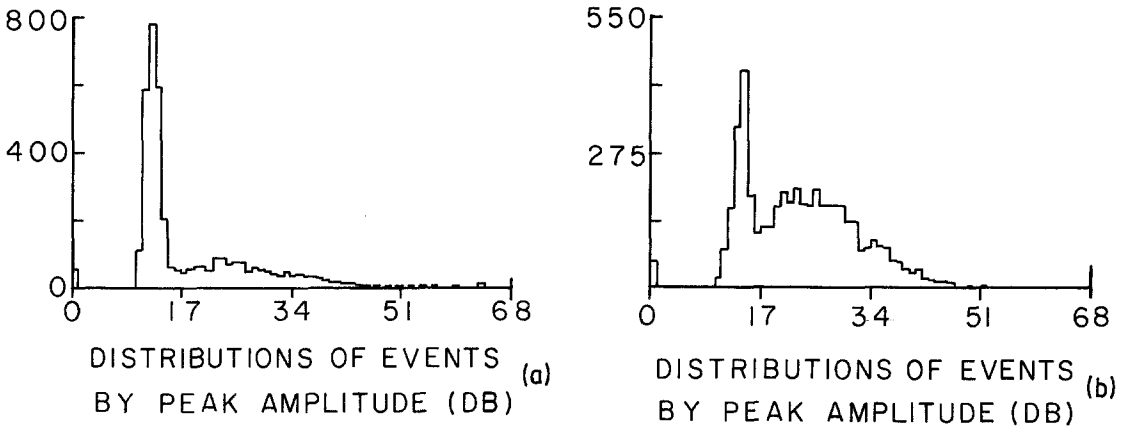

Figure 13 Acoustic emission amplitude distributions obtained under interlaminar loading with the 375 kHz sensor: (a) tensile failure mode; (b) delamination failure mode.

that the relative intensities of the two main peaks (characterizing the amplitude distributions in the respective tests) are different. Although the correlation of the two peaks with a fracture mechanism is not conclusive yet the ratio of their intensities indeed reflected the mode transition around $\phi_f = 0.5$. A fuller account of the acoustic emission data is in preparation [1].

4. Summary

Failure in flexure of PPTA fibre-reinforced epoxy composites occurs by either one of two modes, being tensile and delamination. The fibre volume fraction determines which mode takes place with a transition from tensile to delamination at $\phi_f \approx 0.45$ (for a loading span to depth ratio of 8). Each mode comprises a series of fracture mechanisms, distinguishable by fractographic examinations of the fracture surfaces. A unique example for an observed fracture mechanism is the shearing of an individual Kevlar filament under the delamination mode. The mode transition is reflected in the mechanical properties and in the amplitude distribution of the acoustic emission. Attempts are presently being made to correlate a vast amount of acoustic emission data with the observed fracture mechanisms.

References

1. A. MITTELMAN, M. DAVIDOVITZ, G. MAROM and I. ROMAN, in preparation.
2. H. D. WAGNER, F. R. TULER and G. MAROM, *Polymer* **20** (1979) 653.
3. R. E. ALLRED and N. H. HALL, *Polym. Eng. Sci.* **19** (1979) 907.
4. C. ZWEBEN, *J. Compos. Mater.* **2** (1978) 422.
5. C. C. CHIAO and T. T. CHIAO, "Aramid Fibers and Composites", Lawrence Livermore Laboratory, Preprint UCRL-80400 (1977).
6. C. C. CHIAO, R. L. MOORE and T. T. CHIAO, *Composites* **8** (1977) 161.
7. L. S. PENN and S. M. LEE, *Fibre Sci. Tech.* **17** (1982) 91.
8. R. J. MORGAN, E. T. MONES, W. J. STEELE and S. B. DEUTSCHER, "The Failure Modes and Durability of Kevlar/Epoxy Composites", Lawrence Livermore Laboratory Report Under Contract W-7405-Eng.48.
9. J. H. GREENWOOD and P. G. ROSE, *J. Mater. Sci.* **9** (1974) 1809.
10. R. J. MORGAN, C. O. PRUNEDA and W. J. STEELE, "The Relationship Between the Physical Structure and the Microscopic Deformation and Failure Processes of Kevlar 49 Fibers", Lawrence Livermore Laboratory Preprint UCRL-86802 (1981).
11. M. G. DOBB, D. J. JOHNSON and B. P. SAVILLE, *Polymer* **22** (1981) 960.
12. S. J. DETERESA, R. J. FARRIS and R. G. PORTER, *Polym. Compos.* **3** (1982) 57.
13. C. R. CHAPLIN, *J. Mater. Sci.* **9** (1979) 329.
14. C. A. BERG, J. TIROSH and M. ISRAELI, "Composite Materials Testing and Design" ASTM STP-497 (1971) 206.
15. C. R. CHAPLIN, *J. Mater. Sci.* **12** (1977) 347.
16. T. V. PARRY and A. S. WRONSKY, *ibid.* **16** (1981) 439.
17. M. R. PIGGOTT and B. HARRIS, *ibid.* **15** (1980) 2523.
18. C. W. WEAVER and J. G. WILLIAMS, *ibid.* **10** (1975) 1323.

Received 25 March
and accepted 10 May 1983